AIP Journal of Applied Physics

Chemically guided epitaxy of Rb-irradiated α-quartz

S. Gasiorek, S. Dhar, K. P. Lieb, T. Sajavaara, and J. Keinonen

Citation: Journal of Applied Physics **95**, 4705 (2004); doi: 10.1063/1.1689733
View online: http://dx.doi.org/10.1063/1.1689733
View Table of Contents: http://scitation.aip.org/content/aip/journal/jap/95/9?ver=pdfcov
Published by the AIP Publishing

Articles you may be interested in
Solid-phase epitaxy of silicon amorphized by implantation of the alkali elements rubidium and cesium
AIP Conf. Proc. **1496**, 276 (2012); 10.1063/1.4766542

Light-emitting defects and epitaxy in alkali-ion-implanted α quartz
Appl. Phys. Lett. **88**, 261102 (2006); 10.1063/1.2215615

Cathodoluminescence versus dynamical epitaxy of Ba -ion irradiated α -quartz
Appl. Phys. Lett. **85**, 1341 (2004); 10.1063/1.1784538

Addendum: “Solid phase epitaxial regrowth in ion-beam-amorphized α quartz” [Appl. Phys. Lett. 73, 1349 (1998)]
Appl. Phys. Lett. **74**, 1922 (1999); 10.1063/1.123961

Solid phase epitaxial regrowth of ion beam-amorphized α-quartz
Appl. Phys. Lett. **73**, 1349 (1998); 10.1063/1.122159

[This article is copyrighted as indicated in the article. Reuse of AIP content is subject to the terms at: http://scitation.aip.org/termsconditions. Downloaded to] IP: 137.149.200.5 On: Fri, 21 Nov 2014 20:53:06

HTML ABSTRACT + LINKS

JOURNAL OF APPLIED PHYSICS VOLUME 95, NUMBER 9 1 MAY 2004

Chemically guided epitaxy of Rb-irradiated α-quartz

S. Gąsiorek,[a] S. Dhar, and K. P. Lieb
II. Physikalisches Institut, Universität Göttingen, Tammannstrasse 1, D-37077 Göttingen, Germany

T. Sajavaara and J. Keinonen
Accelerator Laboratory, University of Helsinki, FIN-00014 Helsinki, Finland

(Received 19 August 2003; accepted 3 February 2004)

The solid-phase epitaxial regrowth of 175 keV Rb^+-implanted α-quartz during thermal annealing in air or $^{18}O_2$ was studied as a function of the temperature ($\leqslant$1170 K) and the implanted Rb fluence [$(0.1-6)\times10^{16}$ ions/cm^2]. Rutherford backscattering channeling spectrometry was used to characterize the damage profiles. The role of the oxygen exchange between the annealing gas and the SiO_2 matrix was highlighted by measuring the ^{16}O and ^{18}O profiles by means of time-of-flight elastic recoil detection analysis. Complete epitaxial recrystallization of the amorphized layers was observed after a 1 h annealing in air (at 1170 K) or in $^{18}O_2$ (at 1130 K). The recrystallization rate in air follows a two-step Arrhenius process, with activation energies of 2.7±0.4 and 0.6±0.2 eV above and below an annealing temperature of 1070 K. The three processes, namely, planar recrystallization of the amorphized a-SiO_2 layer, alkali ion out-diffusion, and $^{16}O\Leftrightarrow^{18}O$ exchange, are highly correlated. This correlation is discussed with the help of the concept of the SiO_2 network topology. Finally, the surface topography was measured using an atomic force microscope, which gave evidence of swelling of the SiO_2 matrix during implantation and recompaction during epitaxy.
© *2004 American Institute of Physics.* [DOI: 10.1063/1.1689733]

I. INTRODUCTION

In the current "information age," silicon dioxide in its various crystalline (c) and amorphous (a) forms has a wide spectrum of industrial applications in many technological domains, from microelectronics to photonic switches and nuclear waste storage in glasses.[1,2] The main reasons for the development of SiO_2-based microelectronic components are the excellent chemical, physical, and electronic properties of this matrix. Its doping via ion implantation and the modifications produced thereby are thus very far reaching. Moreover, a fundamental understanding of chemically induced disorder-to-order structural transitions and transport processes in silica is relevant for the synthesis of various technologically important materials, including crystalline α-quartz. Therefore, the knowledge on damage accumulation, amorphization, recrystallization, and the ability to control these processes are indispensable for the future device development.

Recrystallization of ion-beam amorphized α-quartz has been a challenge for decades and has been achieved only quite recently under rather peculiar conditions. For instance, when irradiating natural Brazilian quartz with Si and O ions and post-annealing the samples in air, Devaud *et al.*[3] observed solid-phase epitaxial growth (SPEG) of the matrix to be almost completed at 1320 K. It was concluded that impurity OH groups were responsible for the recrystallization. As early as 1980, Arnold and Peercy[4] had found evidence of the special role of alkali ions during epitaxy in silicates. These authors obtained crystalline $Li_2O\cdot2SiO_2$ when annealing the irradiated sample at 770 K, and recrystallization of Li-doped SiO_2 at 970–1070 K. More recently, Harbsmeier *et al.*[5] carried out similar experiments on pure α-quartz after 50 keV carbon ion implantation and annealing in vacuum up to 1670 K. In these experiments, SPEG was found to set at 1470 K (after C doping). However, no full recrystallization was achieved below 1670 K, the highest annealing temperature used in this experiment. A similar attempt after proton and nitrogen implantations failed.[5,6] Besides these chemically guided SPEG studies, in which implanted or resident impurities play an important role, Dhar, Bolse, and Lieb[7] have achieved full dynamic SPEG after Ne ion implantation and Wang *et al.*[8] after 1.5 MeV Xe ion implantation in hot quartz samples.

Roccaforte *et al.*[9–12] studied chemically guided SPEG of α-quartz after Cs and Na ion irradiation and annealing in air or an $^{18}O_2$ atmosphere. Similar studies after Li implantation were carried out by Gustafsson *et al.*[13] These studies showed full or partial SPEG to occur up to temperatures of about 1170 K. The temperature at which the alkali atoms become mobile and the recrystallization process starts was found to correlate with the fluence and size of the implanted alkali ions. The quality of the regrown crystalline layer improved with the increasing size (Li→Na→Cs) of the alkali ions.[9–14] However, in these studies, the influence of several experimental parameters and the surface morphology was never investigated.

From these observations, SPEG in the presence of Rb ions is expected to be better than the Li or Na ions, and our preliminary results have confirmed this expectation.[15] A more detailed study considering the influence of all experi-

[a]Also at: The Henryk Niewodniczański Institute of Nuclear Physics, ulica Radzikowskiego 152, 31-342 Kraków, Poland; electronic mail: sgasior@gwdg.de

 © 2004 American Institute of Physics

[This article is copyrighted as indicated in the article. Reuse of AIP content is subject to the terms at: http://scitation.aip.org/termsconditions. Downloaded to] IP: 137.149.200.5 On: Fri, 21 Nov 2014 20:53:06

mental parameters has been done now. Here, all these results are presented and compared with the ones obtained previously for Li, Na, and Cs ions.[9–14]

II. EXPERIMENT

High-quality synthetic single-crystalline SiO_2 substrates (α-quartz), (0001) oriented, $10\times10\times1$ mm^3 in size, with one side polished, were mounted on a copper target holder that was kept in thermal contact to a liquid nitrogen reservoir. The samples were irradiated with 175 keV Rb^+ ions to fluences of $(0.1-6)\times10^{16}$ Rb/cm^2 by means of the Göttingen implanter IONAS.[16] The Rb ion energy was chosen to obtain approximately the same projected ion range $R_p\approx100$ nm, as in the previously studied cases of 250 keV Cs^+,[10] 50 keV Na^+,[14] and 15 keV Li^+ implantations.[13] The beam current was kept below 1.5 μA in order to minimize sample heating. Homogeneous implantation over an area of 10×10 mm^2 was achieved via an electrostatic XY sweeping system. The samples were implanted at liquid nitrogen temperature to prevent possible dynamic annealing effects.

Isochronal thermal annealings of 1 or 2 h between 673 and 1173 K were carried out either in air or in an $^{18}O_2$ atmosphere using a furnace from Nabatherm. For annealing in $^{18}O_2$, the samples were enclosed inside quartz ampoules. Each ampoule was evacuated to about 4×10^{-5} mbar and then filled with enriched (98%) $^{18}O_2$ gas; after this the ampoule was sealed. The gas pressure at a particular annealing temperature was set equivalent to the partial gas pressure of oxygen in air at room temperature.

Rutherford backscattering (RBS) and Channeling (RBS-C) spectrometry were used to determine the depth distribution of Rb atoms and the thickness of the amorphous layers by means of a 15 nA beam of 0.9 MeV α-particles. A two-axis goniometer and a surface barrier detector having an energy resolution of 12.5 keV full width at half-maximum, placed at an angle of 165°, were used for these analyses. The RBS data were analyzed by means of the RUMP software package[17] and provided the damage distributions by means of the computer code DAMAGE,[18] which accounts for the dechanneling yield by employing a procedure proposed by Walker and Thompson.[19]

Time-of-flight elastic recoil detection analyses (TOF-ERDA) for depth profiling of the ^{16}O, ^{18}O, Si, and Rb contents were performed at the 5-MV EPG-10-II tandem accelerator of the University of Helsinki.[20] The 53 MeV $^{127}I^{10+}$ beam was directed at 70° relative to the sample normal and the emerging recoils were detected to 70° relative to the sample normal, thus forming a scattering angle of 40° to the incoming beam. The beam current was kept at about 0.5 pnA and the spot size was 1×2 mm^2. The Ziegler–Biersack–Littmark stopping powers[21] and an amorphous density of 2.15 g/cm^3 (6.45×10^{22} at./cm^3) were used for determining the depth distributions. This density is that of ion-beam amorphized SiO_2 and is lower by 19% as compared to the density of α-quartz.[22]

Selected samples annealed in an $^{18}O_2$ atmosphere were examined using atomic force microscopy (AFM) by means of ThermoMicroscopes AutoProbe CP research to analyze the border area between implanted and unimplanted regions.

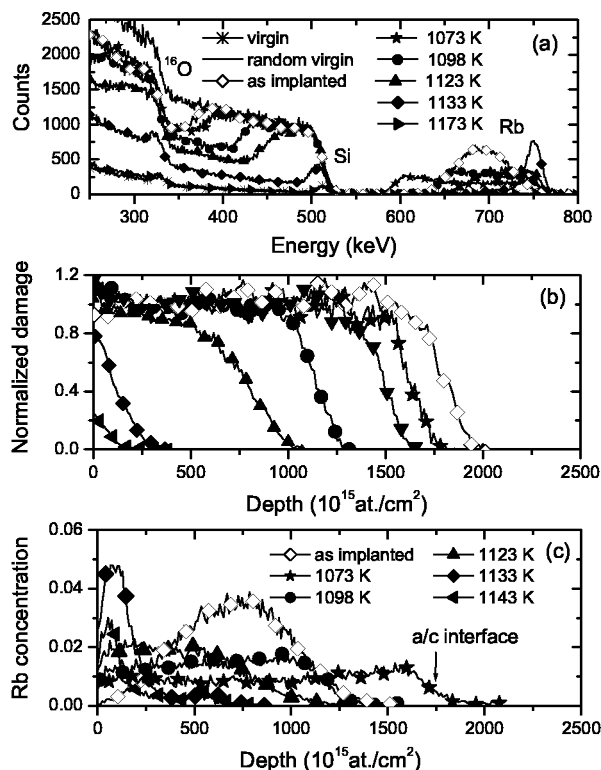

FIG. 1. (a) RBS-C spectra of virgin and Rb^+-ion-irradiated quartz samples at a fluence of 2.5×10^{16} Rb/cm^2 and after annealing in air for 1 h at the different temperatures. (b) Progression of the a/c interface as a function of the annealing temperature. (c) Rb concentration profiles as a function of the annealing temperatures.

III. RESULTS

A. Epitaxy in air

1. Temperature dependence

The influence of the annealing temperature during annealing in air for 1 h was studied for a fixed Rb fluence of 2.5×10^{16} ions/cm^2. The corresponding RBS-C data are reported in Fig. 1(a) and compared with the spectra measured in random (random virgin) and in-channel (virgin) direction in a nonirradiated crystalline sample. The low minimum yield of 5%–7% for the virgin channeling spectrum proved the good quality of the quartz samples. After irradiation, the height of the RBS-C and random spectra agreed to about 380 keV α-energy, indicating the formation of an amorphous layer. Below this energy, the observed channeling yield decreased, revealing the presence of the crystalline substrate underneath the amorphous layer.

From the deduced Si damage profile, as shown in Fig. 1(b), the thickness of the amorphous layer was found to be about 17.8×10^{17} at./cm^2. Using an atomic density of 6.45 $\times10^{22}$ at./cm^3 of a-SiO_2,[22] it was about 280 nm. As shown in Fig. 1(c), the Rb concentration profile of the as-implanted sample had a Gaussian shape, exhibiting its maximum at a depth of $(6.5\pm0.2)\times10^{17}$ at./cm^2. This number is in good

[This article is copyrighted as indicated in the article. Reuse of AIP content is subject to the terms at: http://scitation.aip.org/termsconditions. Downloaded to] IP: 137.149.200.5 On: Fri, 21 Nov 2014 20:53:06

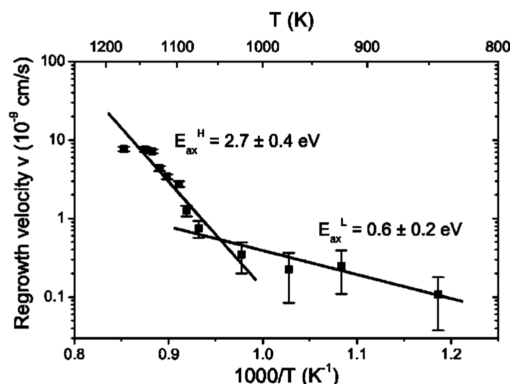

FIG. 2. Recrystallization speed $v(\mathrm{T})$ deduced from Fig. 1(b). The two straight lines correspond to activation energies of $E_{\mathrm{ax}}^L = 0.6 \pm 0.2$ eV (below 1070 K) and $E_{\mathrm{ax}}^H = 2.7 \pm 0.4$ eV (above 1070 K).

agreement with the projected ion range $R_p = 6.47 \times 10^{17}$ at./cm^2 obtained from the TRIM 95 program.[21]

Annealing below 1070 K, the a/c interface hardly moved towards the surface, but the Rb started to migrate throughout the amorphous layer, leading to a box-like Rb profile at 1020 K [see Fig. 1(c)]. At about 1070 K, the a/c front started to move layer by layer towards the surface leaving an epitaxially regrown layer. Parallel to this recrystallization process, the back edge of the Rb profile located near the a/c interface moved. At 1120 K, about half of the amorphous layer had epitaxially recovered and half of the implanted Rb content had diffused out of the sample. At 1170 K, complete SPEG was achieved and the RBS-C spectrum of the recrystallized substrate was identical to that of the virgin one and Rb had completely out-diffused.

From the evolution of the amorphous layer thickness d_a as a function of the annealing temperature, one may extract the regrowth velocity of the a/c interface, $v(T) = \Delta d_a(T)/t$. As shown in Fig. 2, the temperature dependence of the regrowth velocity clearly follows the superposition of two Arrhenius-type exponentials $v(T) = v_o \exp(-E_{\mathrm{ax}}/k_B T)$, where E_{ax} is the activation energy for the recrystallization, v_o the pre-exponential factor, and k_B the Boltzmann constant. A fit to the data yielded the activation energies $E_{\mathrm{ax}}^L = 0.6 \pm 0.2$ eV and $E_{\mathrm{ax}}^H = 2.7 \pm 0.4$ eV in the low and high temperature regimes, respectively (below and above 1070 K). These results suggest different mechanisms in the two temperature regimes.

From the RBS analysis, it was also possible to estimate the activation energy for the Rb out-diffusion during the annealing treatment. The retained Rb fraction plotted in Fig. 3(a) as function of the annealing temperature showed that the Rb content decreased very slowly up to about 1100 K, but then more rapidly with increasing temperature. At $T_{1/2}^{\mathrm{Rb}} = 1130 \pm 60$ K, corresponding to 57% of the melting point of quartz ($T_m = 1983$ K), half the Rb content had left the sample. At 1170 K, Rb had completely out-diffused and full epitaxial recrystallization occurred. In Fig. 3(b), we parametrized the Rb loss in the high temperature range by an Arrhenius dependence, involving an activation energy of $E_{\mathrm{Rb}}^H = 1.5 \pm 0.3$ eV.

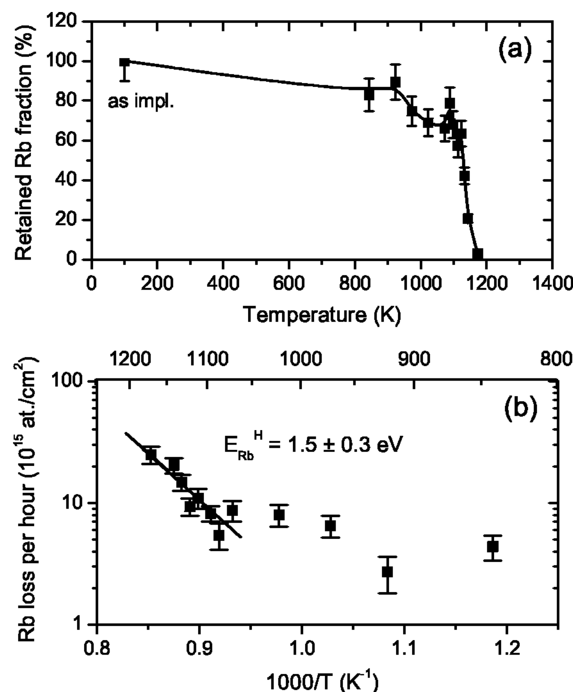

FIG. 3. (a) Retained Rb fraction, integrated up to about 280 nm as a function of the annealing temperature. (b) Rb loss reported as a function of $1/T$.

2. Fluence dependence

In order to find the influence of the Rb fluence on the SPEG process, a set of samples implanted with various fluences were annealed at the fixed temperature of 1123 K for 1 or 2 h. Figures 4(a)–4(c) summarized the results of RBS-C before and after annealing. The initial thickness of the amorphous layer after Rb implantation varied between 16 and 18×10^{17} at./cm^2 for the lowest and highest fluences, respectively, corresponding to 250 and 280 nm.

After annealing of the samples implanted up to the fluence of 1×10^{16} Rb/cm^2 for 1 h, RBS-C spectra [Fig. 4(a)] showed hardly any recovery process. Further annealing for 1 h did not change the situation. However, almost all Rb outdiffused from the sample. Above this fluence, SPEG was clearly visible [Figs. 4(b) and 4(c)] and increased with the annealing time. This clearly demonstrates that there exists a critical Rb content required to intiate the SPEG process. At 2.5×10^{16} Rb/cm^2, more than half of the amorphous layer had recrystallized already after the first hour and the Rb profile started to move towards the surface. After the second hour of annealing, almost complete recrystallization was observed. However, some Rb still remained inside the matrix. For the fluence of $\Phi = 3.4$ and 4.7×10^{16} Rb/cm^2, the channeling spectra after a 1 h anneal were quite close to the virgin spectrum, indicating nearly full recrystallization. After a 2 h anneal, the RBS-C spectra of the fluence 3.4×10^{16} Rb/cm^2 and the virgin sample were indistinguishable, thus confirming the achievement of complete epitaxy. However, for the fluence 4.7×10^{16} Rb/cm^2, the coherent amorphous layer had disappeared, but some isolated damage zones and extended defects due to the presence of Rb ions still remained in the matrix.

[This article is copyrighted as indicated in the article. Reuse of AIP content is subject to the terms at: http://scitation.aip.org/termsconditions. Downloaded to] IP: 137.149.200.5 On: Fri, 21 Nov 2014 20:53:06

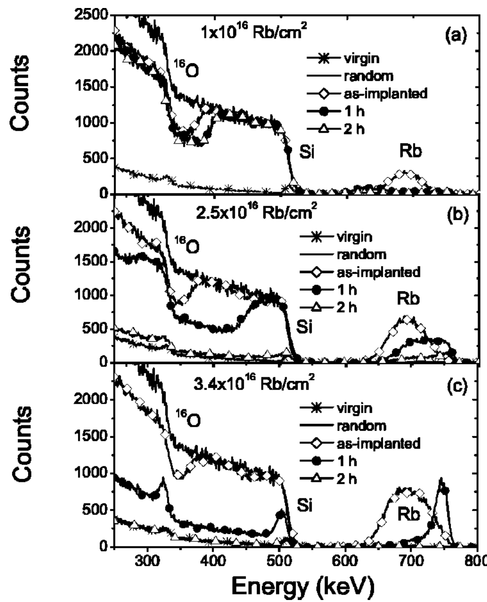

FIG. 4. RBS-C spectra of virgin and Rb^+-ion-irradiated quartz samples before and after 1 h and 2 h annealing at the fixed temperature of 1123 K, measured for Rb fluences of (a) 1×10^{16}, (b) 2.5×10^{16}, and (c) 3.4×10^{16} Rb/cm^2.

From the thickness of the recrystallized layer, the regrowth velocity was calculated after the first and second annealing period and is plotted in Fig. 5 against the integrated Rb content. This velocity depended strongly on the Rb content, reaching a saturation at 3.5×10^{16} Rb/cm^2.

In summary, the constant temperature series at 1123 K showed that full recrystallization of the amorphous/damaged zones in Rb^+-irradiated α-quartz strongly depends on the Rb content and, of course, the annealing time. The SPEG process was accompanied by total out-diffusion of the implanted Rb. There exists a critical fluence of about 1×10^{16} Rb/cm^2 in order to intiate the SPEG process. Above a Rb fluence of about 3×10^{16} Rb/cm^2, SPEG does not work well, even after increasing the annealing time.

B. Epitaxy in $^{18}O_2$ gas

1. Temperature dependence

The measurements of the annealing in $^{18}O_2$ were carried out in order to study the influence of the annealing gas itself

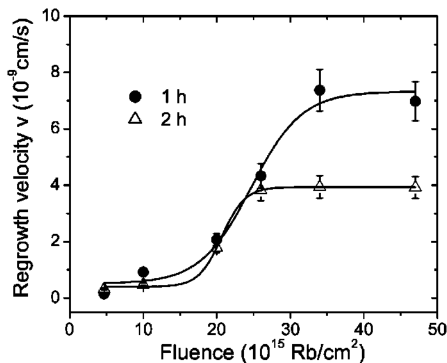

FIG. 5. Regrowth velocity $v(\Phi)$ for 1 h and 2 h annealing at 1123 K as a function of the implanted Rb fluence.

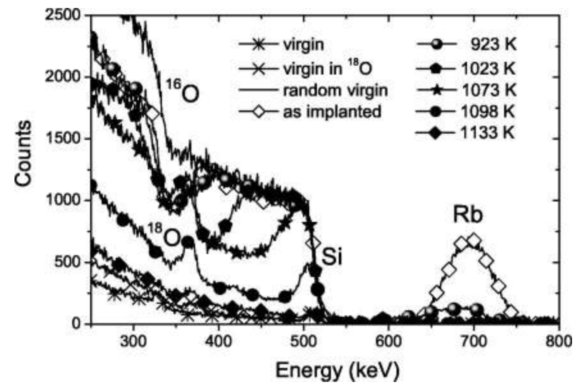

FIG. 6. RBS-C spectra of 175 keV Rb^+-ion-irradiated samples annealed for 1 h in $^{18}O_2$ between 673 and 1173 K.

and the ^{18}O isotope transport into the samples. Rb implantation at a fluence of 2.5×10^{16} ions/cm^2, 1 h isochronal anneals of the samples were performed between 673 and 1173 K. The RBS-C spectra shown in Fig. 6 indicate a layer-by-layer recovery of the amorphous zone for increasing temperature, similar to the case of annealing in air. However, three distinct effects were observed, as compared to the case of annealing in air: (1) a large quantity of external oxygen (^{18}O peak at 360 keV α-particle energy) is transported into the matrix without affecting the stoichiometry of SiO_2, (2) complete SPEG occurred at a lower temperature, and (3) the out-diffusion of Rb was much faster. The regrowth velocity $v(T)$ of the a/c front as a function of the annealing temperature, depicted in Fig. 7(a), follows an Arrhenius dependence. The data suggests a single exponential with an activation energy of $E_{ax}=1.3\pm0.2$ eV.

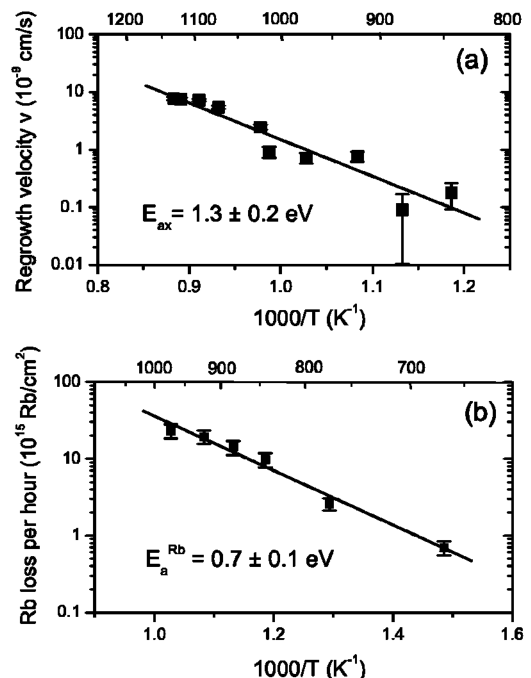

FIG. 7. (a) Arrhenius plot of the regrowth velocity v(T) after annealing in $^{18}O_2$. The straight line corresponds to the activation energy of $E_{ax}=1.3\pm0.2$ eV. (b) Arrhenius dependence of the Rb loss, corresponding to the activation energy $E_a^{Rb}=0.7\pm0.1$ eV.

[This article is copyrighted as indicated in the article. Reuse of AIP content is subject to the terms at: http://scitation.aip.org/termsconditions. Downloaded to] IP: 137.149.200.5 On: Fri, 21 Nov 2014 20:53:06

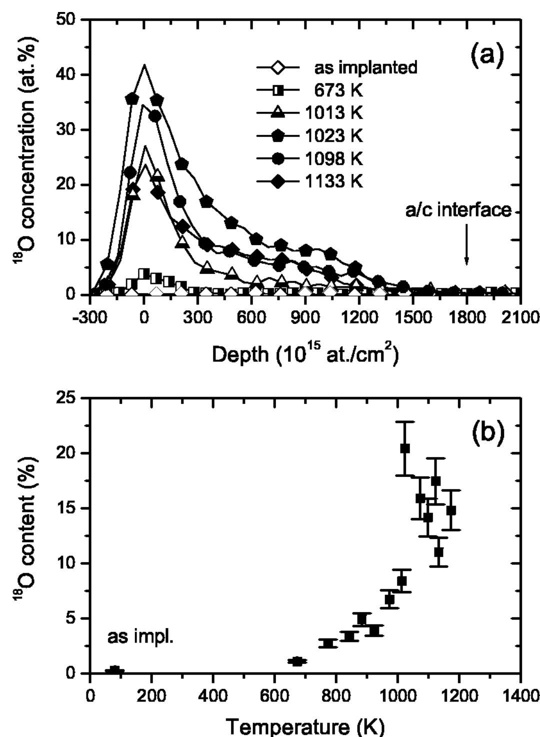

FIG. 8. (a) ^{18}O concentration profiles measured by means of TOF-ERDA for Rb^+-implanted samples, annealed at 673–1133 K for 1 h. (b) ^{18}O content integrated up to the a/c interface, as a function of the annealing temperature.

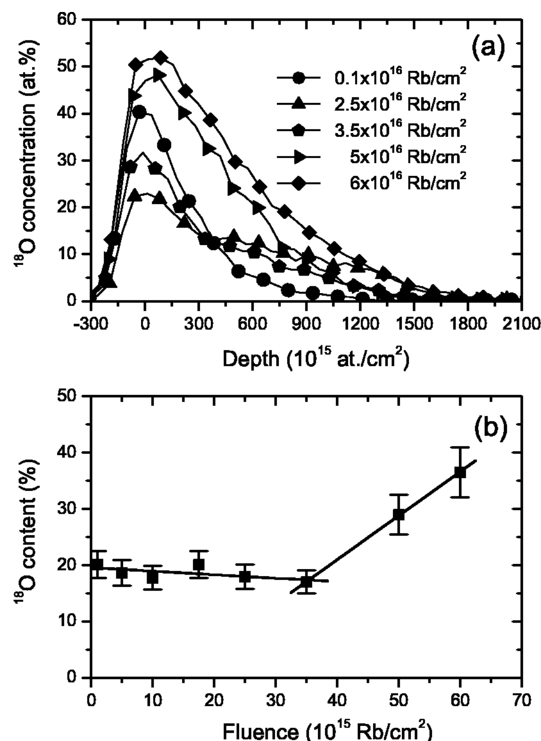

FIG. 9. (a) ^{18}O concentration profiles measured by means of TOF-ERDA for Rb ion fluences of $\Phi=(0.1-6)\times 10^{16}$ Rb/cm^2. The samples were annealed in $^{18}O_2$ atmosphere for 1 h at 1123 K. (b) ^{18}O content integrated up to the a/c interface for different fluences.

The heat treatments at 673–973 K produced a dramatic and rather sudden out-diffusion of Rb. Above 973 K, Rb had totally disappeared from the samples. From the Arrhenius plot of the Rb loss, shown in Fig. 7(b), the activation energy was found to be $E_a^{\mathrm{Rb}}=0.7\pm 0.1$ eV.

From the TOF-ERDA analysis after annealing at different temperatures, the ^{18}O depth distributions in the radiation-damaged zone were obtained and the results are summarized in Fig. 8(a). The $^{18}\mathrm{O}\Leftrightarrow{}^{16}\mathrm{O}$ exchange between the matrix and the annealing gas evidently became stronger with rising annealing temperature. At 673 K, only a very small amount of ^{18}O was detected near the surface. Up to 973 K, the distribution of ^{18}O broadened further near the surface (in the first 50 nm of the amorphous region). After the 1073 K annealing, ^{18}O reached the position of the a/c interface, while beyond the implanted region of about 280 nm the ^{18}O concentration was in accordance with the natural isotope abundance. A large enhancement of ^{18}O was observed (repeatedly) at 1023 K, where SPEG started, and at 1123 K, where almost complete SPEG had been achieved. Figure 8(b) shows the integrated content of the in-diffused ^{18}O as a function of the annealing temperature. It increased with the annealing temperature up to about 1100 K and then saturated. The maximum content was found to be about 15%–20%.

2. Fluence dependence

RBS-C and TOF-ERDA spectra were also taken for samples irradiated with varying Rb^+ ion fluences of up to 6×10^{16} Rb ions/cm^2 and 1 h annealing at 1123 K. The initial amorphous layer thickness (RBS-C spectra are not shown) varied from 15×10^{17} ($\Phi=1\times 10^{15}$ Rb/cm^2) to 19 $\times 10^{17}$ at./cm^2 ($\Phi=6\times 10^{16}$ Rb/cm^2), corresponding to 230–295 nm thick layers. After annealing, the RBS-C spectra of these samples showed similar results as in the case of annealing in air. However, SPEG is much more efficient and Rb out-diffusion is much faster during oxygen annealing.

Figure 9(a) illustrates the ^{18}O concentration profiles for different Rb fluences obtained from TOF-ERDA. It is clearly visible that the $^{18}\mathrm{O}\Leftrightarrow{}^{16}\mathrm{O}$ exchange increases with increasing Rb fluence. This increase is even more distinct in Fig. 9(b), where the total ^{18}O content is plotted as a function of the fluence. The ^{18}O content remained constant up to the fluence of 3.5×10^{16} Rb/cm^2 and then increased linearly. We conclude that the amount of in-diffused oxygen and the quality of the epitaxially recovered layer correlate to some extent with the implanted alkali ion fluence.

C. Surface morphology

The AFM is a useful tool to resolve microscale surface characteristics. In the context of ion implantation and oxygen-induced reactions in quartz, the AFM may also be helpful to verify swelling or compaction phenomena, which are due to amorphization and recrystallization. As the implantation conditions provided a rather sharp boundary between irradiated and nonirradiated regions, the step height Δh at this boundary can be evaluated. As an example, Fig. 10 shows Δh as a function of the annealing temperature. The step height after a fluence of 2.5×10^{16} Rb ions/cm^2 was 24 ± 2 nm. When SPEG set in, the step height started to decrease and finally disappeared at 1133 K, when full epitaxy

[This article is copyrighted as indicated in the article. Reuse of AIP content is subject to the terms at: http://scitation.aip.org/termsconditions. Downloaded to] IP: 137.149.200.5 On: Fri, 21 Nov 2014 20:53:06

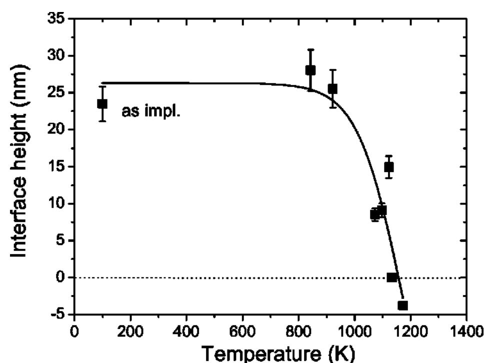

FIG. 10. The height difference Δh at the border area between the implanted and the nonimplanted part of the samples as function of the annealing temperature measured by AFM.

was achieved. At this temperature, the roughness of the recovered surface was slightly larger than that of the nonirradiated one. After annealing at 1173 K, the step height turned out to be slightly negative, suggesting some change of density or loss of material, possibly by evaporation. Thus, the AFM results nicely complement the results obtained via RBS-C analysis.

IV. DISCUSSION

A. Radiation damage

The effects of ion irradiation in α-quartz have been extensively studied both experimentally and theoretically (see, for instance, Refs. 22–29). According to Douillard and Duraud,[26] upon various particle irradiations α-quartz gradually becomes disordered and evolves towards a single amorphous state, which is classified as *metamict*. This amorphous end product is an "optically isotropic, glass-like material with virtually identical density, thermal expansion, and elastic properties."[28] It is almost independent of the irradiation species and is nearly indistinguishable from the end product of ordinary vitreous silica, but has a slightly higher density (by 3%–4%).

The most common and stable phase of all the known polymorphs of SiO_2 at room temperature is α-quartz, which contains three molecular units of SiO_2. The basic structural unit at an ordinary pressure of crystalline and amorphous SiO_2 is the silicon–oxygen tetrahedron $[SiO_4]$. Each $[SiO_4]$ unit is bridged to neighboring tetrahedra via Si–O–Si bonds. All the Si atoms are bonded to four oxygen atoms in such a way that the oxygen atoms are at the corners of the tetrahedron. After ion implantation, a topologically disordered, amorphous network can be formed, which does not exhibit long-range order. However, a-SiO_2 features a rather high degree of structural symmetries as a result of the bonding properties, which is identical to the short-range order of quartz. The theoretical modeling of the network[25,26] assumes that both the crystalline and disordered network are fully connected, all vertices are shared by the maximum possible tetrahedron numbers and there are no nonconnecting tetrahedron corners.

B. Solid-phase epitaxy

Solid-phase epitaxy of quartz after alkali ion implantation and annealing in air/oxygen has been previously studied in the case of Cs and Na implantations.[10–12,14] The main ingredients of this process are recrystallization of the amorphous matrix (via a planar movement of the a/c interface towards the surface), out-diffusion of the alkali ions, and oxygen exchange between the amorphous layer and the annealing gas. The diffusion of alkali ions appears to play an essential role in the SPEG process. The present detailed results after Rb implantations add some important details.

The peculiar influence of Rb ions on the recrystallization process can be understood in terms of the topological SiO_2 network discussed earlier. The Rb ions, which are *network modifiers*,[24,25] are usually considered not to be integrated into the network structure itself, but to occupy interstices within the network,[24] as is the case in alkali-glass silicates. In these silicates,[24,25] oxygen ions of the alkaline oxide introduce nonbridging bonds into the coordination shell of Si, which form complicated chain-like and sheet-like structures of tetrahedral units with bridging oxygen (BO) and nonbridging oxygen (NBO). One oxygen atom is required for the charge balance and is obtained via oxygen exchange from the annealing atmosphere. In all, the alkali-ion-irradiated samples subjected to annealing in $^{18}O_2$, oxygen in-diffusion, and exchange between the matrix and annealing gas were confirmed. The combination of alkali and oxygen ions opens up the network at the position of the BO. The smaller connectivity of the tetrahedral indicates the higher structural freedom of the network and, in comparison to the fully connected network, the tetrahedrons can move and reorient much more easily. It is important to note that the NBO atoms have weaker bond strengths with alkali ions (O–Rb and O–Na: 2.65 eV; O–Cs: 3.06 eV; O–Li: 3.45 eV[30]) than with a Si atom at the center of the tetrahedron (O–Si, 4.57 eV[31]). The more weakly bonded oxygen ions therefore become more easily free under appropriate thermal activation, and the oxygen exchange is favored. This should increase the recrystallizability of the material according to the argumentation of Hobbs *et al.*[25]

C. Alkali ion diffusion

Diffusion of alkali ions in quartz, a-SiO_2, and silicate glasses and the role of defect structures related to impurities or the chemical environment have been studied in much detail and have been reviewed, among others, in Refs. 32–35. Although little is known about Rb diffusion in these materials, as most studies refer to Na diffusion,[33,34,36–42] here, we briefly refer to some results that may elucidate this part of our work.

The non-Debye behavior observed in the electric response of silica and diffusion data has led to the notion of a "forward–backward hopping mechanism" or hopping processes over random potential barriers.[35] Cooperative effects[43] as well as "preferential pathways"[32] governing the dynamics on large scales have been proposed. Recently, molecular dynamics calculations of Na^+ diffusion in $(Na_2O)n(SiO_2)$ (n

[This article is copyrighted as indicated in the article. Reuse of AIP content is subject to the terms at: http://scitation.aip.org/termsconditions. Downloaded to] IP: 137.149.200.5 On: Fri, 21 Nov 2014 20:53:06

$=2,3,4$) silicate glasses[35,44,45] have been compared with neutron scattering measurements.[46]

The diffusion and loss of the implanted Rb ions from SiO_2 can be described by at least three steps: (i) dissolution in the a-SiO_2 network, (ii) "reflection" at the a/c interface due to its very low solubility in crystalline quartz[47] and diffusion towards the surface, and (iii) finally oxide formation and dissociation or evaporation at the sample surface. For this reason, the deduced (effective) activation energies for Rb out-diffusion (E_a^{Rb}) summarize much more complex processes than one would obtain by standard tracer experiments (e.g., after ion implantation or radiotracer in-diffusion). The extracted overall activation energies for annealing in air [$E_a^{Rb}(\mathrm{air}) \approx 1.5 \pm 0.3\,\mathrm{eV}$] or in $^{18}O_2$ [$E_a^{Rb}(^{18}O_2) = 0.7 \pm 0.1\,\mathrm{eV}$], therefore, are very different from the known activation energies for alkali ion diffusion within the a-SiO_2 matrix. For Na diffusion in a-SiO_2, $E_a^{Na} = 1.06\,\mathrm{eV}$ has been found.[48] Diffusion of Cs implanted into an a-SiO_2/Si bilayer studied at 973–1273 K[47] gave the diffusion constant (under nitrogen and in the constraint geometry due to the presence of the SiO_2/Si interface) as $D = 0.5\exp(-2.9\,\mathrm{eV}/k_BT)\,\mathrm{cm}^2/\mathrm{s}$, with $E_a^{Cs} = 2.9\,\mathrm{eV}$. Systematic Na out-diffusion studies under vacuum after implantations in several metals,[41] silicon,[49] and silicon dioxide[42] provided evidence that half the implanted fluence has escaped from the matrix at 58%–70% of the melting temperature, depending on the lattice structure in the crystalline matrices.

D. A scenario for epitaxy

After these preliminary remarks, we may explain the peculiar behavior of Rb^+ ions for SPEG as proposed by Roccaforte and collaborators.[10,11] During annealing, the oxygen diffuses into the a-SiO_2 layer, implanted Rb ions are oxidized and dissolved in the disordered SiO_2 network in the form of $Rb_2^+O^{-2}$; i.e., by forming an alkali glass, in which the BO of the fully connected network are replaced by NBO. In the case of $^{18}O_2$ annealing, a strong correlation between the overall out-diffusion of Rb and ^{18}O migration through the amorphous matrix was observed. The enhancement of the oxygen migration manifests itself by the experimentally observed $^{16}O \Leftrightarrow {}^{18}O$ exchange along "preferred diffusion pathways"[32] of the SiO_2 matrix, which occurs at the broken intertetrahedral linkages (for further details see below). The experimental values of the activation energy for epitaxy is, in all cases, much lower than the Si–O bond energy of 4.57 eV,[31] showing again that the presence of alkali ions and oxygen has a strong influence.

The amount of oxygen migration in the amorphous layer during thermal annealing can be estimated from a simple model proposed by Roccaforte *et al.*[12] In the present case, the migration of Rb ions and in-diffusion of ^{18}O in the SiO_2 layer start at about 770 K. At about 970 K, both Rb and ^{18}O have migrated to the a/c interface. According to this model, it is assumed that each in-diffusing oxygen atom (i.e., each isotope exchange), is accompanied by a "jump" of Rb from one intertetrahedral linkage to another. If we consider the average jump distance ν of the Rb atom as equal to the lattice parameter of SiO_2 along the c axis (i.e., 0.54 nm), then the average number of diffusion steps N_{step} can be estimated from the relation $N_{step} = \lambda/\nu$, where λ is the diffusion length of the Rb ion. At 970 K, the Rb diffusion front at half-maximum has migrated 140 nm towards the c/a interface and 40 nm towards the surface, with respect to the initial Gaussian shape profile. Hence, one can calculate the average Rb migration path $\lambda = 90$ nm. The number of diffusion steps is then given by $N_{step} = \lambda/\nu = 166$. Since the isotope exchange of one oxygen atom is accompanied by the movement of two Rb ions, the total number of oxygen atoms N_o then equals $N_o = 0.5N_{step}N_{Rb}$, where N_{Rb} is the total number of Rb atoms in the network. Using the experimental value of the Rb content in the sample after the annealing at 973 K as obtained from RBS and ERDA, $N_{Rb} = 1 \times 10^{15}\,\mathrm{Rb/cm}^2$, the total amount of the exchanged oxygen amounts to $82 \times 10^{15}\,\mathrm{atoms/cm}^2$. This value is quite close to the experimental integrated ^{18}O content of $84 \times 10^{15}\,\mathrm{atoms/cm}^2$ that was obtained from the ERDA analysis.

E. Comparison with other alkali ions

In the present investigation of Rb-ion-induced damage and recrystallization of α-quartz, the dependence of the epitaxy on the ion fluence and the parameters of the annealing gas (type: air or $^{18}O_2$, temperature, time) was studied in detail. Full or partial epitaxy of the matrix was achieved under properly chosen implantation and annealing conditions. With respect to the results of our previous studies after Li, Na, or Cs implantation the following similarities and differences should be pointed out:

(1) Two main conditions must be fulfilled in order to achieve full epitaxy: the presence of alkali ions and annealing in oxygen. The epitaxy is thought to be a consequence of the dissolution of alkali oxide (network modifiers), which increases the structural freedom of the network due to the formation of nonconneted [SiO_4]-tetrahedron corners, stabilized by nearby alkali ions. The observed correlation between the migration of rubidium and oxygen is used to explain the rearrangement process of the SiO_2 network.

(2) For the typical fluence of $2.5 \times 10^{16}\,\mathrm{Rb\text{-}ions/cm}^2$, full epitaxy was achieved at very similar temperatures in air (1170 K) and $^{18}O_2$ gas (1130 K). The corresponding temperatures after Na and Cs implantations are 920 K (Na, air) and 1150 K (Cs, $^{18}O_2$). For details, see Table I.[10,13,14] Concerning the quality of the epitaxy, Rb turned out to be as profitable as Cs and was definitely much better than Li or hydrogen, for which partial or no epitaxy at all were found.

(3) In the case of Rb implantation, we observed a two-step epitaxy (Arrhenius type) in air and a single-step one in $^{18}O_2$. For air-annealed samples, below 1070 K the deduced activation energy has a value $E_{ax}^L = 0.6 \pm 0.2\,\mathrm{eV}$. Above 1070 K, $E_{ax}^H = 2.7 \pm 0.4\,\mathrm{eV}$. The regrowth rate in $^{18}O_2$ atmosphere can be fitted with a single exponent having an activation energy of $E_{ax}^H = 1.3 \pm 0.2\,\mathrm{eV}$. In the case of Cs implantation, the recrystallization speed was

[This article is copyrighted as indicated in the article. Reuse of AIP content is subject to the terms at: http://scitation.aip.org/termsconditions. Downloaded to] IP: 137.149.200.5 On: Fri, 21 Nov 2014 20:53:06

TABLE I. Processing parameters of chemically guided SPEG in quartz after alkali ion implantation.

Implanted ion type	Energy (keV)	Fluence ($10^{16}/cm^2$)	Annealing gas	$T_{1/2}$ (K)	T_x (K)	E_{ax} (eV)	Ref.
^{1}H	20	5	Air	820(50)	...[a]	...	7, 10
^{7}Li	15	2.5	$^{18}O_2$	875(60)	920[b]	...	10, 13
^{23}Na	50	2.5,5	Air	...	920	...	10, 14
Rb	175	2.5	Air	1130(60)	1170	0.6(2), 2.7(4)	Present work
Rb	175	2.5	$^{18}O_2$	...	1130	1.3(2)	Present work
Cs	250	2.5	Air	1065(50)	1150	2.8(2)	9, 10

[a]No epitaxy.
[b]Incomplete epitaxy.

parametrized by a single activation energy of 2.8 ± 0.2 eV, which is very close to the high-temperature value after Rb implantation in air.

(4) Another similarity occurs for the out-diffusion of the alkali ions from the matrix to its surface. As shown in Table I, the typical temperature, at which half the implanted alkali ion content has left the quartz samples, extends from 820 K for hydrogen and 830 K for Rb (both in $^{18}O_2$) to 1130 K for Rb and 1065 K for Cs (both in air). For Rb and $^{18}O_2$ annealing, the activation energy of this migration process is 0.7 ± 0.1 eV. It thus appears that out-diffusion is less governed by the ion mass than by the annealing oxygen atmosphere. In this context, it would be desirable to measure how the epitaxy and the oxygen and alkali diffusion depend on the gas pressure during annealing.

V. SUMMARY

The present detailed study of chemically guided epitaxy after Rb ion implantation in synthetic α-quartz proves full epitaxy after proper annealing in air or oxygen and demonstrates correlations governing the epitaxial regrowth, the Rb out-diffusion, and the oxygen exchange between the silica matrix and annealing gas. After the irradiation, a continuous amorphous layer grew, which, during epitaxy, decreased in thickness by a planar movement of the a/c interface to the surface. By depth profiling the implanted Rb ions and the $^{18}O\Leftrightarrow^{16}O$ exchange between the sample and the annealing gas, it was possible to monitor the transport of all important partners involved in this process and to relate it to the epitaxy of the matrix. In order to obtain a full picture of the process, measurements at a varying oxygen pressure seem to be desirable. Several similarities and differences among the various alkali ions (Li,Na,Cs) studied so far and between oxygen and air annealing have been found.

ACKNOWLEDGMENTS

Discussions with Prof. W. Bolse and Dr. S. Klaumünzer on the ion irradiation of SiO_2 have been most useful. The authors would like to thank Dr. L. Ziegeler for his help with the $^{18}O_2$ annealing experiments, D. Purschke for his skillful operation of the IONAS heavy ion implanter, and Dr. H. Sepponen for his efficient operation of the tandem accelerator during the TOF-ERDA measurements. This work has been funded by Deutsche Forschungsgemeinschaft (DFG), Deutscher Akademischer Austauschdienst (DAAD), and the Academy of Finland.

[1] G. Roma, Y. Limoge, and S. Baroni, Phys. Rev. Lett. **86**, 4564 (2001).
[2] *Fundamental Aspects of Silicon Oxidation*, edited by Y. J. Chabal (Springer, Berlin, 2001).
[3] G. Devaud, C. Hayzelden, M. J. Aziz, and D. Turnbull, J. Non-Cryst. Solids **134**, 129 (1991).
[4] G. W. Arnold and P. S. Peercy, J. Non-Cryst. Solids **41**, 359 (1980).
[5] F. Harbsmeier, W. Bolse, M. R. da Silva, M. F. da Silva, and J. C. Soares, Nucl. Instrum. Methods Phys. Res. B **136–138**, 363 (1998).
[6] W. Bolse, M. Gustafsson, F. Harbsmeier, and F. Roccaforte, Nucl. Instrum. Methods Phys. Res. B **161–163**, 644 (2000).
[7] S. Dhar, W. Bolse, and K. P. Lieb, J. Appl. Phys. **85**, 3120 (1999).
[8] S. X. Wang, L. M. Wang, and R. C. Ewing, J. Appl. Phys. **81**, 587 (1997).
[9] F. Roccaforte, W. Bolse, and K. P. Lieb, Appl. Phys. Lett. **73**, 1349 (1998); **74**, 1922 (1999).
[10] F. Roccaforte, W. Bolse, and K. P. Lieb, J. Appl. Phys. **89**, 3611 (2001).
[11] F. Roccaforte, S. Dhar, F. Harbsmeier, and K. P. Lieb, Appl. Phys. Lett. **75**, 2903 (1999).
[12] F. Roccaforte, F. Harbsmeier, S. Dhar, and K. P. Lieb, Appl. Phys. Lett. **76**, 3709 (2000).
[13] M. Gustafsson, F. Roccaforte, J. Keinonen, W. Bolse, L. Ziegeler, and K. P. Lieb, Phys. Rev. B **61**, 3327 (2000).
[14] S. Dhar, S. Gąsiorek, M. Lang, K. P. Lieb, J. Keinonen, and T. Sajavaara, Surf. Coat. Technol. **158–159**, 436 (2002).
[15] S. Gąsiorek, S. Dhar, and K. P. Lieb, Nucl. Instrum. Methods Phys. Res. B **193**, 283 (2002).
[16] M. Uhrmacher, K. Pampus, F. J. Bergmeister, D. Purschke, and K. P. Lieb, Nucl. Instrum. Methods Phys. Res. B **9**, 234 (1985).
[17] L. R. Doolittle, Nucl. Instrum. Methods Phys. Res. B **15**, 227 (1986).
[18] J. Conrad, program DAMAGE, Ph.D. thesis, Universität Göttingen, 1996.
[19] R. S. Walker and D. A. Thompson, Nucl. Instrum. Methods **135**, 489 (1976).
[20] J. Jokinen, J. Keinonen, P. Tikkanen, A. Kuronen, T. Ahlgren, and K. Nordlund, Nucl. Instrum. Methods Phys. Res. B **119**, 533 (1996).
[21] J. F. Ziegler, J. P. Biersack, and U. Littmark, in *The Stopping and Range of Ions in Solids* (Pergamon, New York, 1985), Vol. 1.
[22] F. Harbsmeier and W. Bolse, J. Appl. Phys. **83**, 4049 (1998).
[23] *Ion Beam Modification of Insulators*, edited by G. W. Arnold and P. Mazzoldi (Elsevier, Amsterdam, 1987) p. 195.
[24] P. K. Gupta and A. R. Cooper, J. Non-Cryst. Solids **123**, 14 (1990).
[25] L. W. Hobbs, Nucl. Instrum. Methods Phys. Res. B **91**, 30 (1994); J. Non-Cryst. Solids **192/193**, 79 (1995); L. W. Hobbs, A. N. Sreeram, C. E. Jesurum, and B. A. Berger, J. Non-Cryst. Solids **116**, 18 (1996).
[26] L. Douillard and J. P. Duraud, J. Phys. III **6**, 1677 (1996).
[27] W. Bolse, Nucl. Instrum. Methods Phys. Res. B **141**, 133 (1998); **148**, 83 (1999).
[28] F. Piao, W. G. Oldham, and E. E. Haller, J. Non-Cryst. Solids **276**, 61 (2000).
[29] K. P. Lieb, in *Encyclopedia of Nanoscience and Nanotechnology*, edited by N. Malva (in press).
[30] *CRC Handbook of Chemistry and Physics*, edited by D. R. Lide (CRC Press, Boca Raton, FL, 1997–1998).

[This article is copyrighted as indicated in the article. Reuse of AIP content is subject to the terms at: http://scitation.aip.org/termsconditions. Downloaded to] IP: 137.149.200.5 On: Fri, 21 Nov 2014 20:53:06

[31] M. Lamkin, F. Riley, and R. Fordham, J. Eur. Ceram. Soc. **10**, 347 (1992).
[32] M. D. Ingram, Phys. Chem. Glasses **28**, 215 (1987); Philos. Mag. B **60**, 739 (1989).
[33] D. E. Day, J. Non-Cryst. Solids **21**, 343 (1976).
[34] G. H. Frischat, Phys. Chem. Glasses **25**, 110 (1984); W. Beier and G. H. Frischat, J. Non-Cryst. Solids **73**, 113 (1985).
[35] P. Jund and R. Jullien, Philos. Mag. A **79**, 223 (1999); P. Jund, W. Kob, and R. Jullien, Phys. Rev. B **64**, 134303 (2001).
[36] V. F. Antyushin, B. I. Sysoev, and V. F. Syronov, Phys. Status Solidi A **56**, K91 (1979).
[37] V. S. Gerasimenko and A. Yu. Posudievskii, Ukr. Fiz. Zh. **26**, 2030 (1981).
[38] H. Jain, Phys. Status Solidi A **80**, K15 (1983).
[39] N. G. Stenina, L. Sh. Bazarov, M. Ya. Shcherbakova, and R. I. Mashkovtsev, Phys. Chem. Miner. **10**, 180 (1984).
[40] K. B. Hitt and J. J. Martin, J. Appl. Phys. **54**, 5030 (1983).
[41] M. Uhrmacher and K. P. Lieb, Nucl. Instrum. Methods Phys. Res. B **68**, 175 (1992).
[42] G. N. Greaves, J. Non-Cryst. Solids **71**, 203 (1985); Miner. Mag. **64**, 441 (2000).
[43] M. Schwickert, K. P. Lieb, W. Bolse, M. Gustafsson, and J. Keinonen, Nucl. Instrum. Methods Phys. Res. B **147**, 238 (1999).
[44] B. J. Fishbein and J. D. Plummer, Appl. Phys. Lett. **50**, 1200 (1987).
[45] P. Maass, A. Bunde, and M. D. Ingram, Phys. Rev. Lett. **68**, 3064 (1992).
[46] J. Horbach, W. Kob, and K. Binder, Philos. Mag. B **79**, 1981 (1999); Chem. Geol. **174**, 87 (2001); Phys. Rev. Lett. **88**, 125502 (2002).
[47] A. Meyer, H. Schober, and D. B. Dingwell, Europhys. Lett. **59**, 708 (2002).
[48] L. Rybach and F. Laves, Geochim. Cosmochim. Acta **31**, 539 (1967).
[49] V. Milman, M. C. Payne, V. Heine, R. J. Needs, J. S. Lin, and M. H. Lee, Phys. Rev. Lett. **70**, 2928 (1993).

[This article is copyrighted as indicated in the article. Reuse of AIP content is subject to the terms at: http://scitation.aip.org/termsconditions. Downloaded to] IP: 137.149.200.5 On: Fri, 21 Nov 2014 20:53:06